J Fluoresc (2012) 22:163–174
DOI 10.1007/s10895-011-0943-y

ORIGINAL PAPER

Photophysical and Analyte Sensing Properties of Cyclometalated Ir(III) Complexes

Bethany B. H. Leavens · Carl O. Trindle · Michal Sabat · Zikri Altun · James N. Demas · B. A. DeGraff

Received: 27 February 2011 / Accepted: 28 July 2011 / Published online: 10 August 2011

Abstract The synthesis of some heteroleptic, cyclometalated iridium(III) complexes is described. The utility of these $[Ir(ppy)_2(N\text{-}N)]Cl$ (ppy=2-phenylpyridine and N-N= substituted bipyridine, biquinoline, or phenanthroline) complexes as luminescence-based sensors is assessed. The emission intensity of an Ir(III) complex featuring the 3,3′-$H_n$dcbpy ligand ($H_n$dcbpy=dicarboxylic acid-2,2′-bipyridine; n=0,1,2 to indicate deprotonated, mono- and diprotonated species, respectively) is seen to increase in the presence of Pb(II). Insight into the structure and analyte-sensing capability is achieved by X-ray crystallography in conjunction with computational modeling. Complexes incorporating carboxylic acid-functionalized bipyridine and biquinoline as the polypyridyl ligand show pH sensitivity while similar phenanthroline complexes do not.

Keywords Iridium(III) · Orthometallated · Luminescence · Lead detection · Iridium complexes · Theoretical state calculations

B. B. H. Leavens · C. O. Trindle · M. Sabat · J. N. Demas (✉)
Chemistry Department, University of Virginia,
Charlottesville, VA 22904, USA
e-mail: demas@virginia.edu

M. Sabat
Nanoscale Materials Characterization Facility,
Department of Materials Science and Engineering,
University of Virginia,
Charlottesville, VA 22904, USA

Z. Altun
Physics Department, Marmara University,
Göztepe Kampus, Kadiköy,
Istanbul, Turkey

B. A. DeGraff
Chemistry Department, James Madison University,
Harrisonburg, VA 22807, USA

Introduction

The attractive photophysical properties of many d^6 transition metal complexes have prompted study into their potential utility in a wide variety of applications. Much of this work has been focused on luminescent complexes of Ru(II), which are valued for their facile synthesis, relative photostability, and wide applicability [1, 2]. Ruthenium polypyridyl complexes, along with complexes of less-commonly used transition metals such as Re(I) and Os(II), have been incorporated as luminescence-based sensors for a variety of analytes [3]. Prior work has shown that Ru(II) and Re(I) complexes incorporating the 3,3′-Hdcbpy ligand exhibit an increase in quantum yield in the presence of Pb (II). However, the quantum yields, particularly in the latter case, are not very high [4, 5].

The synthesis and study of highly-luminescent cyclometalated iridium(III) complexes have brought about great interest in recent years [6]. Most notably, their use as dopants in organic light emitting diodes (OLEDS) has dramatically increased the efficiency of these devices [7]. Examples of bis- and tris- cyclometalated Ir(III) complexes with relatively high quantum yields and lifetimes of several

microseconds are not uncommon [8]. In spite of their attractive photophysical properties, however, relatively little is known about the utility of cyclometalated iridium(III) complexes as luminescence-based sensors. This work was to explore their potential utility as strongly emissive pH and metal ion sensors.

Many factors govern the photophysical properties of a luminophore [4]. In the relatively new field of luminescent Ir(III) complexes, there is much yet to be determined. The nature of the excited states of $[Ir(ppy)_2(N\text{-}N)]^+$ (ppy=2-phenylpyridine and N-N=and substituted bipyridine, biquinoline, or phenanthroline) complexes have been discussed to some degree, although uncertainties remain [9]. The effects of polypyridyl ligand choice on bis-cyclometalated iridium(III) complexes are examined here in order to assess their potential use as sensors. Given the difficulty of designing and synthesizing new useful ligands and getting X-ray structures of some complexes, we conducted computational studies to see what such modeling can tell us about structures and sensor responses of new molecules. This should guide the synthesis of molecules with specific sensing properties.

Experimental

Materials All solvents were reagent grade and used as received. The 3,3′-H_2dcbpy ligand was prepared according to a literature procedure and the structure and purity were established by NMR and melting point [10]. ^{1}H NMR (CD_3OD, 300 MHz δ=7.353 (2 H; 5,5′), 7.942 (2 H; 4,4′), 8.370 (2 H; 6,6′). MP=260 °C (lit=262 °C). The 4,4′-dcbpy ligand was purchased from Alfa Aesar. The 4,4′-biquinoline ligand was purchased from Aldrich. The 4,7-dihydroxy-1,10-phenanthroline was purchased from GFS Chemicals and purified by methanol extraction. The 5-hydroxy-1,10 phenanthroline ligand was prepared from a literature procedure [11] as was the 5-N$(Bu)_2$ ligand [12]. $IrCl_3$ was purchased from Aesar.

$[(ppy)_2IrCl]_2$ was synthesized as previously reported [13]. All $[Ir(ppy)_2(N\text{-}N)]Cl$ complexes were synthesized according to well-established methods involving other polypyridyl ligands [14]. In contrast to prior procedures, however, the purification was carried out via acid-washed alumina column. Eluents, added sequentially to each successive elution, were as follows: acetone, methanol (up to 15%), acetic acid (up to 5%), and trifluoroacetic acid (up to 2%). The structure of the polypyridyl ligand used in each complex is shown in Fig. 1.The studied complexes include $[Ir(ppy)_2(3,3'\text{-dcbpy})]Cl$ (**1**), $[Ir(ppy)_2(4,4'\text{-dcbpy})]Cl$ (**2**), $[Ir(ppy)_2(4,4'\text{-biquinoline})]Cl$ (**3**), $[Ir(ppy)_2(5\text{-OH-1,10-phenanthroline})]Cl$ (**4**), $[Ir(ppy)_2(4,7\text{-OH-1,10-phenanthroline})]Cl$ (**5**), and $[Ir(ppy)_2(5\text{-N}(Bu)_2\text{-1,10-phenanthroline})]Cl$ (**6**).

Luminescence Measurements Luminescence and excitation spectra were measured on a Spex Fluorolog 2+2 spectrofluorometer. Lifetime measurements were done on a Laser Science VSL 337 pulsed N_2 (337 nm) laser decay system. Data fitting of the decays to a sum of exponentials was performed using nonlinear least-squares routines in Mathcad [15] or PsiPlot [16].

All pH titrations were carried out with roughly 10 μM Ir (III) complex in 0.1 M phosphate buffers. The pH titration for **3** was carried out in 50:50 water:methanol to facilitate solubility. To enhance the luminescence intensities, Pb(II) titrations were carried out in acetone. The Pb(II) titration was carried out by adding aliquots of an acetone solution of lead acetate to a 10 μM solution of complex **1** in acetone. The lead(II) solution contained an equivalent concentration of the Ir(III) complex such that the concentration of the luminophore was unchanged to avoid dilution corrections.

Calculations We found structures for all species with the help of Amsterdam Density Functional (ADF2008.01) software [17]. Structural results reported here derive from geometry optimizations with the local density approximation (LDA) to the density functional and a Slater-type triple-zeta polarized (TZP) basis set; for the metals a "small"-sized pseudopotential core was adopted. We investigated gradient-corrected PBE functionals as well with the TZP and TZ2P basis sets, and found virtually identical structures (bond distances within 0.02 Angstroms). The "pure" (nonhybrid) gradient-corrected functionals typically produced slightly longer bond distances than the LDA values.

To estimate the absorption spectra we used several different formulations of the time-dependent density functional method, a linear response theory. These include the time-dependent density functional (TD-DFT) linear response method as implemented in ADF with the "statistical average of orbital potentials" (SAOP) model [18] and a TZP basis. For electronic excitations no pseudopotential core was invoked. Using the ADF LDA/TZP structures, we also computed absorption spectra by TD-DFT with Spartan [19] as well as Gaussian 03 [20] and 09 [21] software. In these cases the B3LYP functional was employed. For the metals Spartan used a variant of the Hay-Wadt Los Alamos pseudopotential core and the attendant basis [22] called LACPV* [23]. A 6–31 G(d) basis was placed on other atoms. This produced a 712-member basis for the largest system, $Ir(ppy)_2$3,3'-dcbpyPb(II) monocation. In Gaussian we used B3LYP with the basis sets LANL2MB, LANL2DZ, and a hybrid basis with LANL2DZ on the metals and 6–31 G(d) on other atoms. We call this latter method a B3LYP/hybrid model chemistry. The same basis sets and B3LYP functional were used for TD-DFT modeling of spectra, using a configuration space of 70

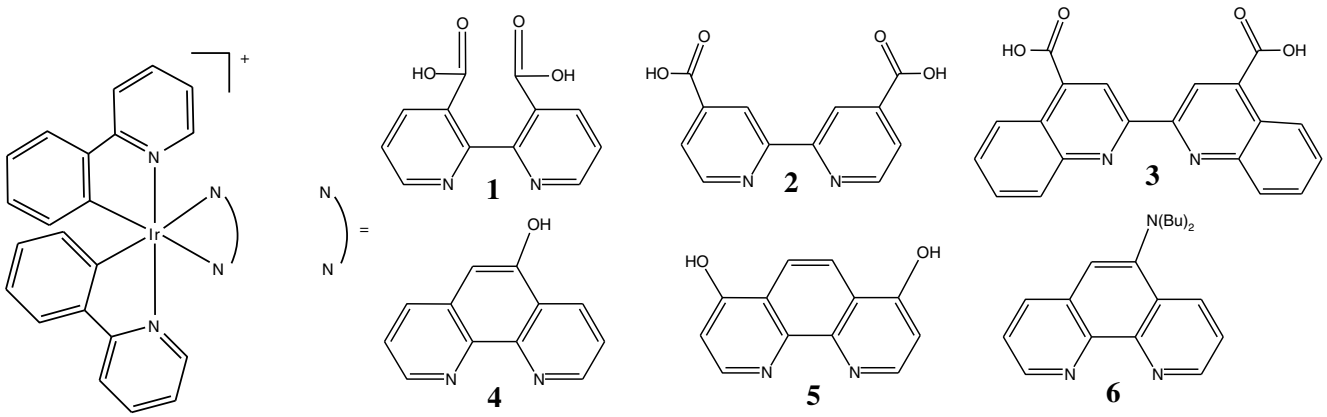

Fig. 1 [Ir(ppy)$_2$(N-N)]Cl complexes. The number by each ligand corresponds to the complex made from that ligand

single excitations. These results were qualitatively identical with the Spartan results; the smaller basis sets predicted excitations shifted to the blue. We were able to treat a larger manifold of excitations in Gaussian; all spectra and MOs reported here were done with Gaussian 09. Solvent effects were modeled by the Polarizable Continuum Model (PCM) of Tomasi [24].

Graphic images of orbitals were produced by modules within ADF, Spartan 08, and Gaussian 09's graphical interface GaussView. Spectra were redrawn from Gaussian data exported from GaussView 5. The reconstituted spectra were produced using normalized Gaussian forms, each with a width of 0.2 eV, centered at the computed transition energy, and weighted by the computed oscillator strength.

X-Ray Structure A thin needle-shaped colorless crystal of complex **1** (approximate dimensions: 0.31×0.10×0.08 mm) was used for a data collection on a Bruker SMART APEX II CCD diffractometer using MoKα radiation. Empirical absorption corrections were applied with the transmission factors ranging 0.402–0.819.

The crystal structure was solved by direct methods in Bruker SHELXTL [25]. The final least-squares refinement with anisotropic thermal displacement parameters for all non-H atoms yielded the R factor of 0.0795 (wR2=0.2022) for 9522 reflections with I>2σ(I). Hydrogen atoms were included in calculated positions without further refinement. The final difference Fourier map showed a peak of the height 1.91e/Å^3 located near the Ir atom.

Results and Discussion

We have been studying transition metal complexes as sensors for both pH and metal ions, especially lead. For lead sensors we have focused on metal complexes containing 3,3′-H$_2$dcbpy (1). Perkovic demonstrated the utility of this ligand on Ru(II) complexes and we have extended the work to Re(I) complexes [4, 5]. For Ru(II) there is a large increase on luminescence quantum yield on Pb(II) complexation, which has been attributed to the increased planarity of the 3,3'-dcbpy ligand on Pb(II) binding. Perkovic was able to obtain the structure for the uncomplexed Ru(II) complexes, but not the Pb(II) complex. Nor have we been able to obtain crystals of the Pb(II) complex with the Ru(II) or related H$_2$dcbpy complexes of Re(I) or Ir(III). In the absence of crystal structures of the lead complex, not only is the increased planarity unproved, but also the structures of the Pb(II) complexes remain a mystery. To test the planarity hypothesis and to determine the structure of the Pb(II) complexes, we have conducted theoretical calculations.

Structural Modeling of Ru(II) Species The structures and photo-physics of ruthenium complexes have been thoroughly studied. We began our modeling project with the well known Ru(II) system that would allow direct comparison of computed and measured properties. We computed the structure of Ru(bpy)$_2$Hdcbpy$^+$ complex using a LDA/TZP model in the ADF program suite for comparison with the known structure [4]. The computed torsion angles for the 3,3'-dcbpy in this complex are NCCN=18.3° and CCCC=26.5°, which compare well with X-ray structure values of 15.3° and 21.1° respectively. This success led us to use the same LDA/TZP method to search for the most stable structure of the Pb(II) complex. Simpler Pb(II) complexes have been thoroughly investigated; Shimony-Livny, Glusker, and Bock [26] observe that all the Pb(II) compounds in the Cambridge Structural Database for which Pb(II) has coordination number 2 to 5 display hemidirected coordination meaning that all four Pb-O bonds are in a single hemisphere. These authors found that MP2/LANL2DZ calculations showed that tetracoordinated Pb(II) complexes with four NH_3, PH_3, AsH_3, SbH_3, and BiH_3 all displayed hemidirection, as did Pb(II) with four OH_2,

SH_2, SeH_2, and TeH_2 ligands. The Pb(II)$(H_2O)_4$ species displayed a C_2-symmetric bisphenoid structure with two Pb-O bonds of lengths 2.46 Å forming an angle of 147°, and two PbO bonds of length 2.36 Å forming an angle of 98°. This is roughly consistent with calculations by Arfa, Olier, and Privat, [27] who found corresponding values of 2.43 Å and 137°, and 2.32 Å and 103° in B3LYP/LANL2DZ modeling. Our corresponding LDA/TZP(medium core) calculation on Pb(II)$(H_2O)_4$ produced values of 2.45 Å and 114° and 2.39 Å and 97° – also consistent with the other estimates. The spread in values suggests that the structure is very soft. That is, the potential function for the torsional coordinate is rather flat so that slight differences in the method can give noticeably different estimates of the location of the minimum. Regardless of the fine details, our LDA/TZP calculations on Pb(II)$(H_2O)_4$ produce the hemidirected structure consistent with other calculations and the known structures. This justifies our use of the base model LDA/TZP to describe the hemidirectional coordination of 4-coordinated Pb(II) in our complexes.

We found a structure for Ru$(bpy)_2$3,3'-dcbpyPb in which the carboxylic acid oxygens form a pocket for the lead. All four carboxyl oxygens are coordinated to lead, and the Pb-O coordination is "hemidirected," as we found for the simpler complexes. The hemidirection and the limitation to coordination number four is robust. Added water does not coordinate to the exposed face of the Pb. This is consistent with the chemistry of lead complexes and theoretical structural calculations described above.

This hemidirectional bonding of lead and the absence of water coordination to the Pb(II) in the complex are consistent features of the structure regardless of which computational method we use. Our LDA/TZP model produces a hemidirected structure for the coordination of lead to carboxyl oxygens in Ru$(bpy)_2$3,3'-dcbpyPb. The two pairs of OPbO angles are very different, 56° and 112°. We attribute the reduction of the larger angle in the complex relative to the Pb(II)$(H_2O)_4$ value to geometric constraints on the position of oxygen atoms. The differences in bond lengths are, however, not as large as in the Pb(II)$(H_2O)_4$ dication. PbO bonds making the smaller angle have bond length 2.36 Å, while the PbO bonds making the larger angle have bond length 2.38 Å.

Binding of lead reduced the NCCN dihedral angle to 14.7° and the CCCC angle to 17.3°. Thus, theoretical results confirm the suggested planarization of the ligand as a consequence of Pb(II) binding and supports the explanation for the enhanced luminescence on lead binding with the Ru(II) complex as a consequence of the change in torsion angle. The coherent picture of the Ru(II) structures gives some assurance that modeling can profitably be applied to the analogous but more complex Ir(III) complexes described below.

Structural Modeling of Ir(ppy)$_2$3,3′-Hdcbpy Since Ir(III) complexes are frequently much more highly luminescent than Ru(II) and Re(I) complexes, and thus may serve as a more sensitive Pb(II) detector, we examined Ir$(ppy)_2$3,3'-Hdcbpy and its binding to Pb(II). All prior attempts at obtaining a crystal structure of the iridium complex with the 3,3′-dcbpy ligand capturing Pb(II) have been unsuccessful [4, 5], so we constructed a computational model of the 3,3′-Hdcbpy Ir(III) system and its response to Pb(II) binding. Geometric parameters including the primary bond lengths, bond angles, and even the torsion angle of the ring-ring twist of the neutral Ir(III) (Pb-free) species agree fairly well with the crystal structure.

The crystal structure (Fig. 2) shows that the geometry of the complex is roughly octahedral. No counterion is present so one carboxylic group of the 3,3′-dcbpy ligand must be deprotonated to maintain charge balance. The NCCN torsion angle about the 2,2′ axis of the substituted bipyridine ring for complex **1** is 29.7°, which is substantially larger than the 18.3° for the Ru(II) complex. By analogy to the response of Ru(II) complex to Pb(II) capture, it seemed likely that the substituted bipyridine ligand of the Ir(III) complex should be similarly planarized on Pb(II) binding and should sense Pb(II) as the Ru(II) complex does.

Table 1 shows a comparison of selected geometric parameters for the neutral dicarboxylic acid species obtained by X-ray crystallography with those calculated by geometry optimization applying a variety of computation methods. Bond distances R are expressed in Å, angles in degrees. The C-C* bond connects the substituted pyridyl fragments in the 3,3'-Hdcbpy ligand. The torsion angles are twists around this CC* link.

Details of the computed geometry vary with the computational model, and depart in some cases from the X-ray values. Gradient corrected (PBE) and hybrid functional (B3LYP) produce longer metal-N and pyridyl-pyridyl

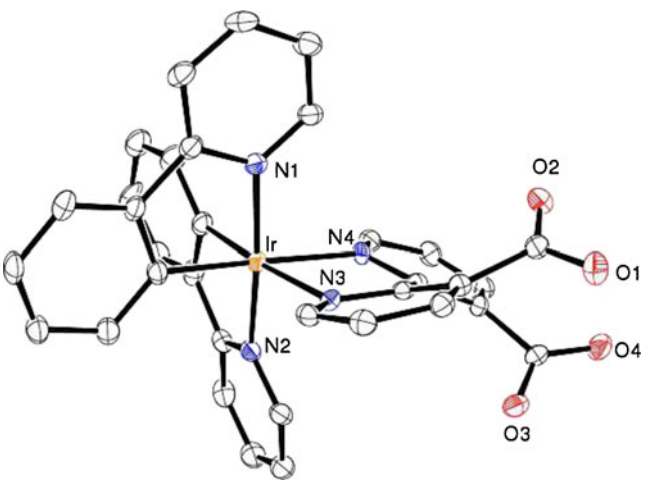

Fig. 2 ORTEP drawing of Complex 1, 30% probability ellipsoids

Table 1 Geometric parameters for Ir(ppy)$_2$3,3'-Hdcbpy

Parameter	X-ray	LDA/TZP	PBE/TZP	B3LYP/hybrid	B3LYP/hybrid:H_2O
R(Ir-N)	2.153, 2.167	2.137, 2.141	2.217, 2.227	2.210, 2.209	2.175, 2.182
R(N-C)	1.354, 1.349	1.348, 1.356	1.373, 1.362	1.356, 1.367	1.344, 1.352
R(C-C)*	1.491	1.467	1.489	1.493	1.469
R(C-C)	1.398, 1.407	1.399, 1.400	1.412, 1.416	1.413, 1.408	1.398, 1.398
R(C-COO)	1.517,1.524	1.549, 1.499	1.567,1.521	1.567, 1.497	1.525, 1.480
R(C-O) anion	1.256, 1.259	1.240, 1.252	1.256, 1.256	1.242, 1.260	1.251, 1.252
R(C-O) neutral	1.204, 1.322	1.209, 1.341	1.216, 1.360	1.216, 1.352	1.217, 1.349
Torsion CCCC	34.5	32.5	37.1	32.5	33.2
Torsion NCCN	29.7	28.6	32.7	27.0	26.4

Lengths are in Angstroms and angles are in degrees.

Optimizations were conducted with a PCM representation of methanol solvent.

bond distances than the local density functional (LDA) predicts. Computation predicts distinct C-COO bond lengths for the carboxylates, 1.56±0.01 Å and 1.51± -0.01 Å , while the X-ray structure has these distances very nearly equal., 1.52±0.01 Å. This suggests that one of the carboxyl groups is protonated while the other is not, but we were unable to support this in the modeling. In modeling we found a structure in which the proton links essentially equivalent carboxyl groups by a hydrogen bond. This is calculated to be more stable than structures in which the carboxyl groups are distinct, but inconsistent with the X-ray structure's significantly different carboxyl bond lengths. Protonating one carboxyl and H-bonding a water molecule to the unprotonated carboxyl group (described in the column labeled B3LYP/hybrid:H_2O) does not change the bond lengths of the complex significantly (mean absolute deviation in this set relative to the X-ray values remains between 0.015 and 0.016 Å.) However, it does have an impact on the computed torsion angle. The calculations tend to overestimate the dihedral angle, but values computed for the B3LYP/hybrid and B3LYP/hybrid:H_2O structures bracket the experimental values.

Structural Effect of Pb(II) Binding Ir(ppy)$_2$3,3'-Hdcbpy and Ir(ppy)$_2$3,3'-dcbpyPb$^+$ as modeled with the LDA/TZP, PBE/TZP and B3LYP/hybrid model chemistries both have approximately C_2 symmetry. All methods give quite consistent descriptions. The structure of Ir(ppy)$_2$3,3'-dcbpyPb(II) from B3LYP/hybrid and PBE/TZP models is shown in Fig. 3. In the lead complex, lead coordinates with all four carboxylic oxygens; consistent with the constrained geometry and with a general pattern observed in four-coordinated lead complexes, the coordination is in one hemisphere. Coplanarity is much enhanced in the dicarboxylic acid-substituted bipyridyl attending Pb(II) complexation. In PBE/TZP, the NCCN angle decreases from 32.7° for the neutral IrdcH system to 22.6 for the Ir3,3'-dcbpyPb(II) system, while in the B3LYP/hybrid model the torsion angle NCCN is reduced from 27.0° to 20.5°. Because the potential defining equilibrium torsion angle is likely to be quite soft, we consider these estimates to be reasonably consistent. Clearly lead binding increases planarity as expected. The Pb-O distances in the lead-bound system alternate between two slightly longer and two slightly shorter values, 2.37 and 2.35 Å in PBE/TZP and 2.364 and 2.351 Å in B3LYP/hybrid. We have explored the placement of waters around the lead, but find there is little tendency to add waters to the lead atom, already hemi coordinated by the four carboxylic oxygens, again consistent with the preferred structures of lead complexes discussed above.

As Pb(II) dication is bound, the CCCC torsion angle defining the 3,3'-dcbpy ring-ring twist decreases from 34° in the dicarboxylic acid to about 25° in the lead dicarboxylate. The carboxylic acid oxygens in the neutral system define a severely puckered ring (ring torsion angle tau=49°). Pb(II) binding reduces this angle to 35°. The O-O distances in the dicarboxylic acid are 2.25 Å (within a carboxyl group) and 3.40 Å (between carboxyl groups). Again, these results illustrate planarization of the 3,3′-dcbpy ligand on lead complexation. We should note the shortening of Ir-N bond lengths as Pb is bound. This must also enhance the ligand field strength, which could have an impact on the spectra.

Figure 3 shows the binding mode for the Pb(II) to the 3,3'-dcbpy. The staggering and inequivalence of the carboxylate oxygens are clearly visible. The greatly increased planarity and reduced distortion on lead binding are clear. The Ru(II)- Pb(II) complex has a similar staggered structure.

Independent modeling with the ADF software suite, using pure density functionals LDA (no gradient correction) and PBE (gradient corrected) with the TZP basis produces comparable values for these geometric parameters. For the dicarboxylic acid, the values obtained in ADF for the

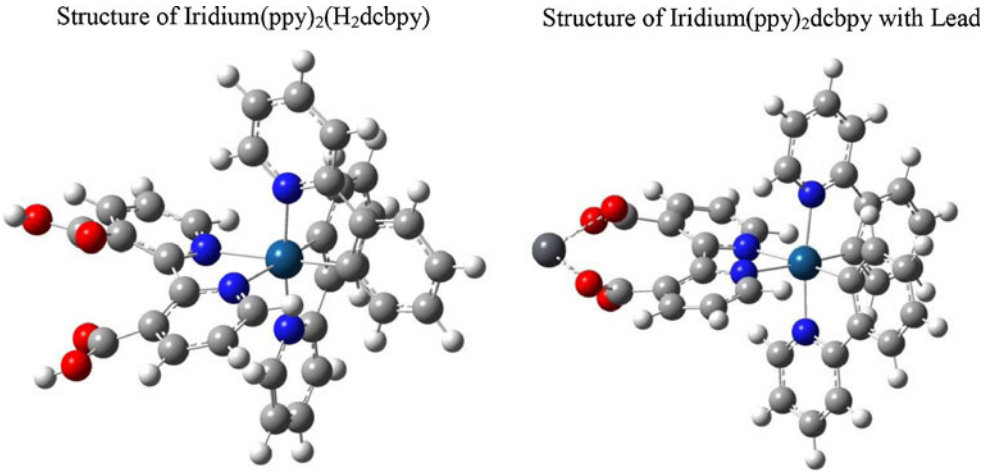

Fig. 3 Molecular model of binding of Pb(II) to complex 1

torsion angles bracket the values quoted above within 2°. The O-O distances within a carboxylic acid fragment bracket the values quoted above and are within 0.02 Å of the values obtained by the B3LYP/hybrid model. The distances between O atoms in different carboxylic acid fragments are less well defined owing to easy twisting, but again as Pb(II) is bound we see a substantial shortening of the O-O distances. Thus, for ground state structures, the LDA/TZP, PBE/TZP, and B3LYP/hybrid calculations all lead to reasonable results.

We thought that calculations would allow an estimate of the energy of Pb(II) binding, but getting reasonable calculated energies proved difficult. For the ruthenium capture of Pb^{2+} we may write the reaction

$$\mathrm{Ru(bpy)_2H_2}3,3'\text{-dcbpy}^{2+}\text{: S} + \mathrm{Pb(H_2O)_4^{2+}}\text{: S} \rightarrow \mathrm{Ru(bpy)_2}3,3'\text{-dcbpyPb}^{2+}\text{: S} + 2\mathrm{H_2O}\text{ : S} + 2\mathrm{H_3O^{1+}}\text{: S}$$

Here S refers to some kind of solvent model. While structural calculations described above incorporated no model of solvent, the energy calculations for reactions of charged and polar systems in polarizable medium require recognition of solvent effects. In the absence of medium effects, the value of the energy change of this reaction as written is +57 kcal/mol as estimated by the model chemistry B3LYP/hybrid and including no consideration of solvent. However if the products are taken to be the $H_5O_2^{1+}$ strongly H-bonded fragments, the reaction energy is −26 kcal/mol.

The simplest treatment of the solvent (methanol) is provided by the polarizable continuum model. If all species in the reaction as written above are taken to be immersed in the polarizable continuum (using methanol's dielectric constant) the reaction energy becomes +86 kcal/mol. However, if the species in methanol is assumed to be $H_5O_2^{1+}$, the reaction energy is +27 kcal/mol. None of these models of the solvent is plausible, since the specific H-bonding interaction of water and hydronium with the methanol medium is neglected. A more detailed treatment of the solvent is required for a realistic estimate of the energetics. We have considered a process in which the solvent model includes clusters of six methanols, which then solvate the separated product waters and hydronium. The reaction energy for this elaborate model is −5.3 kcal/mol.

We have conducted similar calculations for the reaction of $Ir(ppy)_2$3,3'-Hdcbpy(H_2O):S with $Pb(H_2O)_4^{2+}$:S The most elaborate model of the medium, involving methanol clusters, produces a reaction energy of +24 kcal/mol. We cannot claim however that this treatment of the methanol medium is the last word, or that the computed reaction energies are reliable.

Proper treatment of the medium is clearly necessary but very difficult. As our results show, the energies are highly sensitive to the model and more elaborate modeling is necessary. Published studies of methanol clusters with water and hydronium ion are extensive [28] and exceedingly complex [29]. The largest systems systematically treated by electronic structure modeling so far have no more than four methanols [30].

Computed Spectra We have modeled absorption spectra for the $Ru(bpy)_3^{2+}$ and $Ir(ppy)_2$bpy cation, as well as the dicarboxyl substituted species and the Pb(II) complexes. For the species with carboxylic acid ligands, we found that the SAOP/TZP model produced quite unrealistic descriptions of spectra without inclusion of solvent. The predicted low-energy transitions were far too red with some low lying transitions involving charge transfer from the metal to the carboxylates, an unlikely process. When solvent effects were incorporated into the model, these anomalous transitions moved to high energies and out of the spectroscopic range of interest. In keeping with the literature [31], we use the TD-B3LYP/hybrid computations for all of the spectra reported here, and incorporate solvent effects through the PCM representation of acetone or methanol.

Once again we take the well-studied Ru(II) systems as a reference by which we can judge the adequacy of our calculations. The HOMOs and LUMOs of the Ru(II) and Ir (III) complexes with the 3,3′-dcbpy ligand are shown in Figs. 4 and 5, respectively. As is widely accepted in the literature, the lowest energy transitions in the Ru(II) complexes are between orbitals that are largely pure d states to π* states, although the LUMOs do contain some d character.

While the Ru(II) HOMO is largely metal-d, the HOMO of the Ir(III) complex contains substantial π character from the phenylpyridine ligands as well. The Ir(III) lowest lying transitions are a strong mixture of d-π to π*. Thus, they involve a substantial component of interligand π-π* character. This mixed d and π character on the initiating orbitals no doubt accounts in part for the complexity of the spectroscopy of these and other Ir(III) complexes relative to similar Ru(II) complexes.

Figures 6 and 7 show the computed absorption spectra of $Ru(bpy)_2$3,3'-Hdcbpy and $Ir(ppy)_2$3,3'-Hdcbpy and their lead complexes. We do not include the individual state energies and intensities as about 70 different transitions with complex orbital parentage are used in the calculation.

The spectra are all in reasonable agreement with the experiments. Table 2 shows the calculated and observed data. The calculations reproduce the positions of the ligand localized π → π* well including the molar extinction coefficients, which are typically only about 25% low. The visible near uv metal-ligand charge transfer transitions are less consistent, but generally too blue by typically 2000–3000 cm^{-1}. For Ru(II) complexes their shifts with lead complex are in reasonable agreement with the experimental [4, 32], although the red shifts attending Pb(II) binding are exaggerated for both Ru(II) and Ir(III). Especially with the Ir complexes it is difficult to make unambiguous assignment because of their complexity. For example Ir(ppy) $phen^+$ has a continuum of shoulder from the visible to about 300 nm. If one takes the center of this group as the state energy, the agreement is similar to the other complexes. Again the molar extinction coefficients are about 30% low. The agreement in band intensities is quite remarkable, as we had expected this to be one of the more difficult quantities to calculate well. The orbital parentages are all reasonable. As expected from the orbital picture, the low-lying Ir(III) transitions contain a significant interligand π → π* contribution along with the MLCT component.

We consider the reason for the increased luminescence on Pb(II) binding. In the lead free complex, the 3,3'-Hdcbpy is highly strained and distorted from planarity. The interpretation is that the strained ligand has a lower effective crystal field strength than planar bpy ligands [4, 33]. A lower crystal field lowers the d-d state energies, which permits more efficient quenching of the luminescence through thermal activation. Lead coordination has been assumed to drive the ligand toward greater planarity with a concomitant increase in crystal field strength that will raise the d-d state, reduce quenching, and account for the enhanced luminescence.

Our calculations strongly support the assumption that Pb (II) binding increases the planarity of the dcbpy. Resolution of the question of the effect on increased planarity of the ligand on the d-d states is much more complex. To locate the d-d states, we examined the basis sets and states with energies below 42 kcm^{-1} (>240 nm), but found no essentially pure d → d transitions for either the Ru or the Ir complexes. There was some d character for the virtual MOs for both Ru and Ir complexes, but mixing with ligand MOs is extensive. In particular, the LUMOs for both the Ru (II) and Ir(III) species are comprised mainly of π* (3,3′-dcbpy). The findings for the HOMO and LUMO of **1** are consistent with characterization of similar $[Ir(ppy)_2(N\text{-}N)]^+$ species [9]. Thus, trying to ascertain the locations of the purported d-d states responsible for the quenching of the emission in the ligand field quenching model does not seem to be currently possible.

Structure of the Triplet State Since the emission is commonly considered to originate in the triplet T_1, we

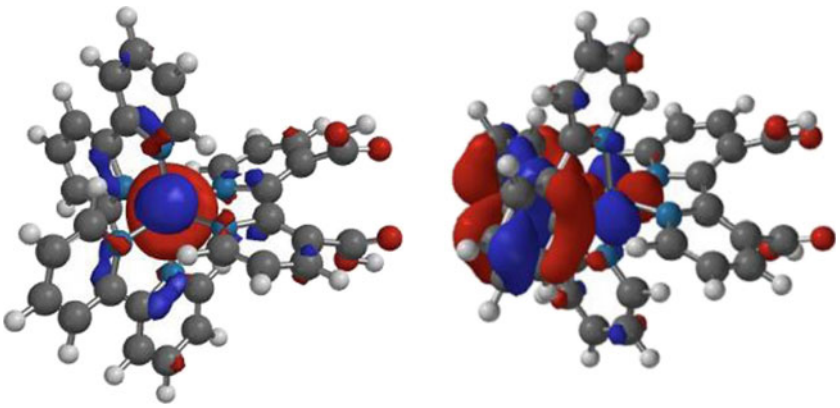

Fig. 4 HOMOs of $[Ru(bpy)_2(3,3'\text{-dcbpy})]^{2+}$ (left) and $[Ir(ppy)_2(3,3'\text{-dcbpy})]^+$ (right)

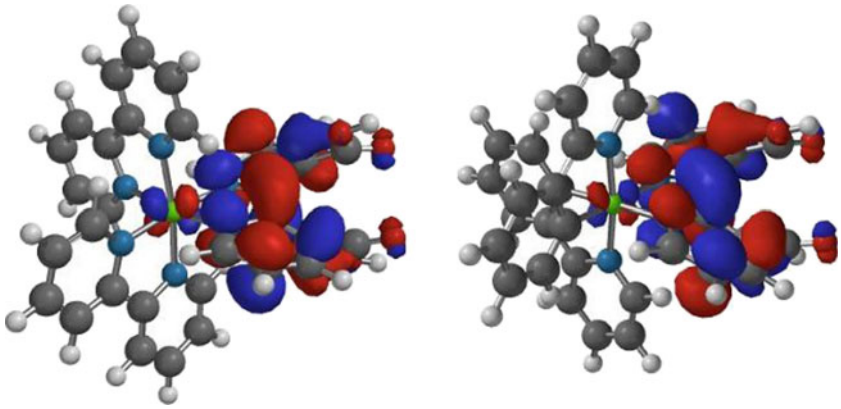

Fig. 5 LUMOs of $[Ru(bpy)_2(3,3'\text{-dcbpy})]^{2+}$ (left) and $[Ir(ppy)_2(3,3'\text{-dcbpy})]^{+}$ (right)

optimized the structure of the triplets for DCH-water and DC-Pb in the B3LYP/hybrid scheme, with PCM representation of methanol solvent (Table 3). The structure of the DCH-water system triplet is significantly altered from the ground singlet; besides alterations in the bond lengths of the substituted bpy (consistent with the occupation of the former LUMO), the torsion angle is considerably reduced. Coordination of Pb^{2+} nearly equalizes the C-O bond distances; as in the singlet, the hemicoordinated Pb has nearly equal bond distances to the carboxylic oxygens. Significantly, the torsion angle is appreciably reduced by Pb binding in the triplet as well as the singlet species. We note that the Ir-N shortening observed for the singlet as Pb is bound does not occur in the triplet. The triplet state energy for the DCH-water case is 1.90 eV; this is consistent with the broad emission. The value for the Pb-coordinated system is 1.68 eV, suggesting a red shift in the emission as Pb is bound.

Experimental Results In both the Ir(III) and the Ru(II) systems, the lowest excited state directly involves the binding carboxylic acid groups, which may influence the Pb(II) ion sensitivity. In the accepted model of changes in the crystal field strength, the more muted Ir(III) results could be attributed to a stronger crystal field of Ir vs. Ru with a concomitant greater energy gap between the emitting level and the lowest quenching d-d state, which results in a smaller sensitivity to change in ligand planarity. Unfortunately, due to the extensive mixing of d and π character in the excited states, there is no clear way to ascertain what are actually d states in the simple model. Thus, we cannot rule out or support the d-d quenching model for Pb(II) sensing with our calculations.

While Ir complex **1** senses lead, the Pb(II) effect on the luminescence quantum yield is muted compared to analogous Ru(II) and Re(I) complexes, and the luminescence quantum yield is disappointingly low compared to other orthometallated Ir(III) complexes. Figure 8 depicts the change in emission intensity versus concentration of Pb (II). Though the fractional change is rather small, the titration curve demonstrates a clear increase in quantum yield with increasing Pb(II) concentration. Fitting of this intensity data yields an association constant K_{ass} of ca $0.1 \pm 0.05\ \mu M^{-1}$, which is an order of magnitude less than that of the analogous Re(I) complex. This poorer binding can probably be attributed to the much larger distortion from planarity and the inability of the Pb(II) binding to torque the ligand into a more favorable binding

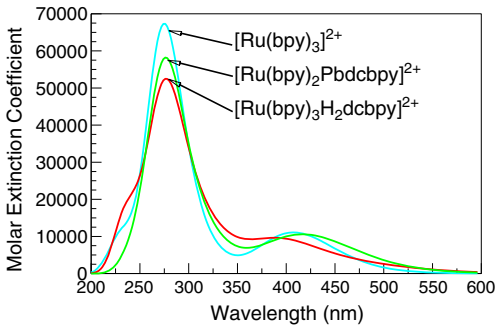

Fig. 6 Computed spectra of the Ru(II) complexes

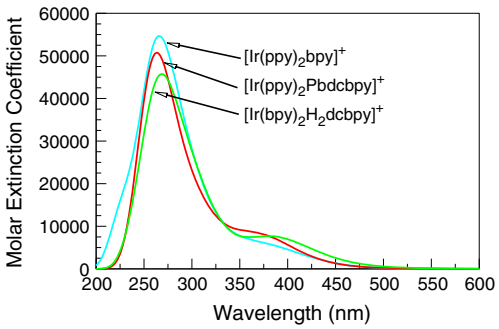

Fig. 7 Computed spectra of the Ir(III) complexes

Table 2 Comparison of experimental and theoretical wavelengths for absorptions

Complex		Ligand transitions	CT/LL transitions
		Wavelength (nm)	
$[Ru(bpy)_3]^{2+}$	Experimental	287	454
	Theoretical	274	404
$[Ru(bpy)_2H_23,3'\text{-dcbpy}]^{2+}$	Experimental [4]	299	452
	Theoretical	276	388
$[Ru(bpy)_2Pb3,3'\text{-dcbpy}]^{2+}$	Experimental [4]	288	458
	Theoretical	266	416
$[Ir(ppy)_2phen]^{+}$	Experimental [32]	252, 265 sh	303 sh, 337 sh, 412 sh, 464 sh
	Theoretical	264	380
$[Ir(bpy)_23,3'\text{-}H_2dcby]^{+}$	Experimental	282	372, 452 sh
	Theoretical	262	370
$[Ir(bpy)_2Pb3,3'\text{-dcby}]^{+}$	Experimental	266	372
	Theoretical	Not measured	386

configuration. Similarly, the lifetime of the complex in acetone, 83 ns in the uncomplexed form increases to 99 ns in the presence of Pb(II). In contrast $[Ir(ppy)_2(bpy)]Cl$ showed no change in emission intensity or lifetime, even at Pb(II) concentrations orders of magnitude greater than that of the Ir(III) complex. This result is consistent with the lack of a lead-binding site, and shows that Pb(II) is not a quencher of the excited state.

Figures 9 and 10 show pH titration data, respectively, for Ir(III) complexes **2** and **3**. The data sets are fit according to previously derived equations [34]. The acid dissociation constants for **2** determined from the fits using two sequential protonations are 3.3 and 4.4, and that obtained for complex **3** using a single protonation is 3.4. It was somewhat unexpected that the data from the complex incorporating the 4,4′-dicarboxylic acid biquinoline ligand would be most accurately fit with a one-proton model, given the two protonation sites on the ligand and the use of a two-proton model for the similar bipyridyl complex. This trend can be explained if one pK_a of the complex is lower than the range tested or if the lifetime of the complex does not change with one of the two protonations.

Complex **2** demonstrates a change in quantum yield with pH; however, the overall quantum yield was observed to be low in water or mixed solvent systems containing as little as <10% water. Complex **3** incorporating the biquinoline ligand was synthesized in an effort to improve upon the low quantum yield, but the same solvent-dependent quenching behavior was observed. Solvent-dependent emissive behavior in $[Ir(ppy)_2(N\text{-}N)]^{+}$ complexes has been previously described [35], but

Table 3 Structural parameters for $Ir(ppy)_2dcbpy$ singlets and triplets [a]

Parameter	B3LYP/hybrid-water Singlet Ground State	B3LYP/hybrid-water Triplet	B3LYP/hybrid-Pb Singlet Ground State	B3LYP/hybrid-Pb Triplet
R(Ir-N)	2.175, 2.182	2.191, 2.199	2.210, 2.209	2.204, 2.184
R(N-C)	1.344, 1.352	1.396, 1.394	1.356, 1.367	1.403, 1.405
R(C-C*)	1.469	1.432	1.493	1.445
R(C-C)	1.398, 1.398	1.449, 1.443	1.413, 1.408_{COO}	1.454, 1.456
R(C-COO)	1.525, 1.480	1.519, 1.474	1.567_{COO}, 1.497	1.485, 1.479
R(C-O) anion	1.251, 1.252	1.264, 1.265	1.242, 1.260	1.284, 1.280, 1.277, 1.280
R(C-O) neutral	1.217, 1.349	1.223, 1.360	1.216, 1.352	
R(O-Pb)			32.5	2.352, 2.371, 2.380, 2.363
Torsion CCCC	33.2	20.2	27.0	10.3
Torsion NCCN	26.4	19.1	2.210, 2.209	13.1

Lengths are in Angstroms and angles are in degrees.

Optimizations were conducted with a PCM representation of methanol solvent.

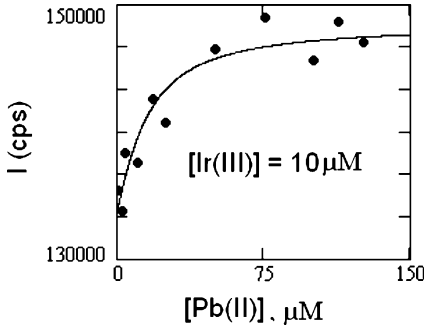

Fig. 8 Effect of Pb(II) on emission intensity of complex 1 in acetone. The solid line is the best fit to a 1:1 binding mode with K_{ass}=0.1 μM^{-1}

the magnitude of the red shift and intensity decrease upon addition of water suggests an interaction of the water with the carboxylic acids specific to **1**–**3**. Figure 11 shows the effect of even small amounts of water on **1**.

Complexes **4, 5,** and **6** were tested for pH sensitivity. Over the pH range 2–10 there were no emission changes. $[Ir(ppy)_2(1,10\text{-phenanthroline})]^+$ complexes with substituents at the 5- or 4-and 7-positions of the phenanthroline ligand are widely known to show remarkably diverse emissive behavior, both in terms of emission energy and quantum yield. Low-temperature spectra indicate that the emission of analogous complexes can arise from a combination of Ir(III) → phenanthroline, Ir(III) → ppy, and π → π* (phenanthroline) transitions. With complexes **4**–**6**, it is our belief that the electron donating -OH or -N $(Bu)_2$ groups on the phenanthroline ligand raise the energy of the MLCT (phenanthroline) transition such that it is not the dominant emission. Consequently, chelation of protons by this polypyridyl ligand will not bring about significant changes in the emission spectra.

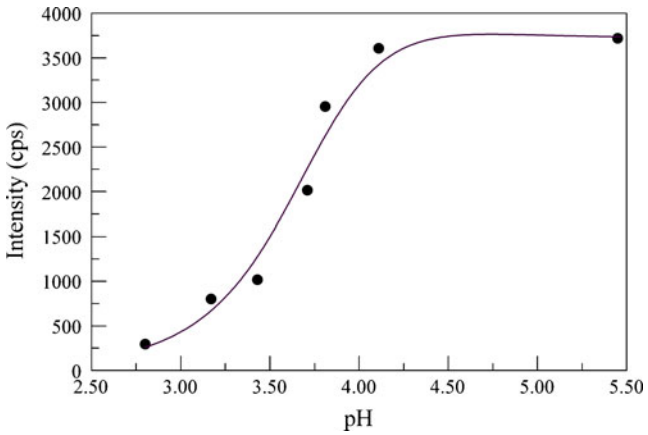

Fig. 9 Intensity-based pH titration of complex 2. The solid line is the best fit assuming two sequential protonations with pK1=3.3 and pK2=4.4

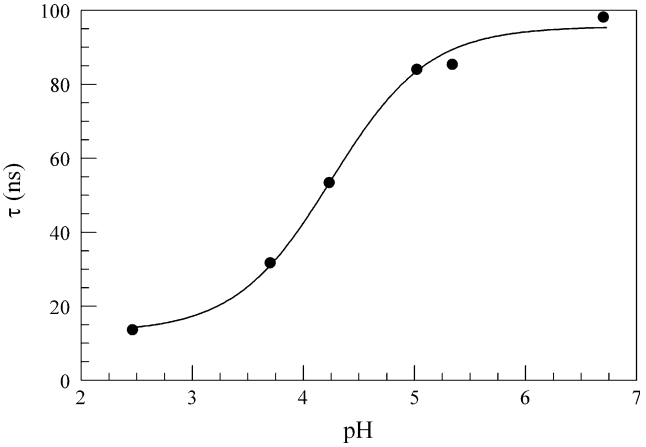

Fig. 10 Lifetime-based pH titration of complex 3. The best fit pK is 3.4 for a single step protonation

Conclusions

We have assessed the applicability of $[Ir(III)(ppy)_2(N\text{-}N)]$ complexes in lead and pH sensing applications. The luminescence and sensing behavior are highly sensitive to the substituent on the polypyridyl ligand but not in a cleanly predictable fashion. Further, in contrast to the usual high luminescence efficiency and long lifetimes of ortho-metallated Ir(III) complexes, the complexes studied were disappointingly short lived and inefficient.

Molecular modeling has proved a robust method for determining the structures of the 3,3'-dcbpy complexes bound to Pb(II) whose structures were previously unknown. Our results confirm the predicted increased planarity on Pb (II) binding. Calculations provide insight into the spectroscopy properties of the excited states of the complexes and their relationship to sensing properties. However, the excited state manifolds are too complex for us to unambiguously locate the d-d excited state necessary to confirm their predicted involvement in the lead sensing ability of 3,3'-dcbpy complexes. Calculations also demon-

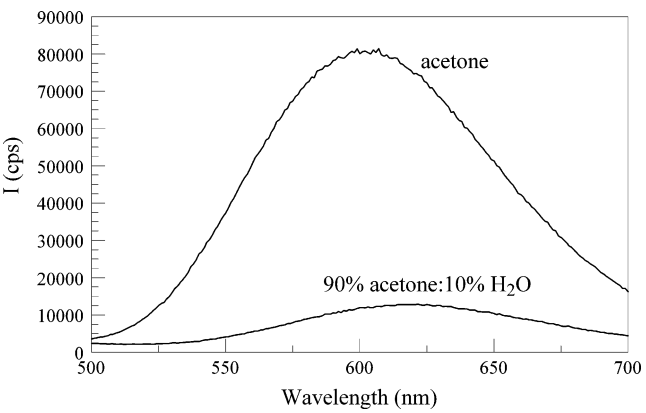

Fig. 11 Effect of water on emission intensity of complex 1

strated the large excited state distortions that have been proposed for MLCT excited state of metal complexes.

Acknowledgments We gratefully acknowledge the support of NSF grant CHE 04–10061 and the University of Virginia Chemistry Department. Marmara University's Research Fund (BABKO) provided essential support for Zikri Altun. Carl Trindle gives thanks to the Body Foundation for support of travel, and to the Department of Chemistry, UVa for computer equipment. B. A. DeGraff gratefully acknowledges the support of the Dreyfus Foundation.

References

1. Jain A, Xu W, Demas JN, DeGraff BA (1998) Binding of luminescent ruthenium(II) molecular probes to vesicles. Inorg Chem 37(8):1876–1879
2. Xu H, Aylott JW, Kopelman R, Miller TJ, Philbert MA (2001) A real-time ratiometric method for the determination of molecular oxygen inside living cells using sol−gel-based spherical optical nanosensors with applications to rat C6 glioma. Anal Chem 73(17):4124–4133
3. Demas JN, DeGraff BA (1991) Design and applications of highly luminescent transition metal complexes. Anal Chem 63 (17):829A–837A
4. Perkovic MW (2000) Allosteric manipulation of photoexcited state relaxation in $(bpy)_2Ru(II)$(binicotinic acid). Inorg Chem 39 (21):4962–4968
5. Hueholt BB, Xu W, Sabat M, DeGraff BA, Demas JN (2007) Structure and luminescence properties of monomeric and dimeric Re(I) complexes with dicarboxylic acid-2,2′-bipyridine ligands. J Fluor 17(5):522–527
6. Sajoto T, Djurovich PI, AB Tamayo, Oxgaard J, William A, Goddard I, Thompson ME (2009) Temperature dependence of blue phosphorescent cyclometalated Ir(III) complexes. J Am Chem Soc 131(28):9813–9822
7. Kim JI, Shin I-S, Kim H, Lee J-K (2005) Efficient electrogenerated chemiluminescence from cyclometalated iridium(III) complexes. J Am Chem Soc 127(6):1614–1615
8. Zhao Q, Jiang C-Y, Shi M, Li F-Y, Yi T, Cao Y, Huang C-H (2006) Synthesis and photophysical, electrochemical, and electrophosphorescent properties of a series of iridium(III) complexes based on quinoline derivatives and different β-diketonate ligands. Organometallics 25(15):3631–3638
9. DeAngelis F, Fantacci S, Evans N, Klein C, Zakeeruddin SM, Moser J-E, Kalyanasundaram K, Bolink HJ, Grätzel M, Nazeeruddin MK (2007) Controlling phosphorescence color and quantum yields in cationic iridium complexes: a combined experimental and theoretical study. Inorg Chem 46(15):5989–6001
10. Dholakia S, Gillard RD, Wimmer FL (1985) 3,3′-dicarbomethoxy-2,2′-bipyridyl complexes of palladium(II), platinum(II) and rhodium(III). Polyhedron 4(5):791–795
11. Shen Y, Sullivan BP (1995) A versatile preparative route to 5-substituted-1,10-phenanthroline ligands via 1,10-phenanthroline 5,6-epoxide. Inorg Chem 34(25):6235–6236
12. Slough GA, Krchňák V, Helquist P, Canham SM (2004) Synthesis of readily cleavable immobilized 1,10-phenanthroline resins. Org Lett 6(17):2909–2912
13. Sprouse S, King KA, Spellane PJ, Watts RJ (1984) Photophysical effects of metal-carbon.sigma. bonds in ortho-metalated complexes of iridium(III) and rhodium(III). J Am Chem Soc 106(22):6647–6653
14. Neve F, Crispini A, Campagna S, Serroni S (1999) Synthesis, structure, photophysical properties, and redox behavior of cyclometalated complexes of iridium(III) with functionalized 2,2′-bipyridines. Inorg Chem 38(10):2250–2258
15. http://www.ptc.com/products/mathcad/
16. http://www.polysoftware.com/plot.htm
17. ADF2009.01, SCM, Theoretical Chemistry, Vrije Universiteit, Amsterdam, The Netherlands, http://www.scm.com
18. Schipper PRT, Gritsenko OV, van Gisbergen SJA, Baerends EJ (2000) Molecular calculations of excitation energies and (hyper) polarizabilities with a statistical average of orbital model exchange-correlation potentials. J Chem Phys 112:1344–1352
19. Shao Y, Molnar LF, Jung Y, Kussmann J, Ochsenfeld C, Brown ST, Gilbert ATB, Slipchenko LV, Levchenko SV, O'Neill DP, DiStasio RA Jr, Lochan RC, Wang T, Beran GJO, Besley NA, Herbert JM, Lin CYeh, Van Voorhis T, Chien SH, Sodt A, Steele RP, Rassolov VA, Maslen PE, Korambath PP, Adamson RD, Austin B, Baker J, Byrd EFC, Dachsel H, Doerksen RJ, Dreuw A, Dunietz BD, Dutoi AD, Furlani TR, Gwaltney SR, Heyden A, Hirata S, Hsu C-P, Kedziora G, Khalliulin RZ, Klunzinger P, Lee AM, Lee MS, Liang WZ, Lotan I, Nair N, Peters B, Proynov EI, Pieniazek PA, Rhee YM, Ritchie J, Rosta E, Sherrill CD, Simmonett AC, Subotnik JE, Lee Woodcock H III, Zhang W, Bell AT, Chakraborty AK, Chipman DM, Keil FJ, Warshel A, Hehre WJ, Schaefer HF III, Kong J, Krylov AI, Gill PMW, Head-Gordon M (2006) Advances in methods and algorithms in a modern quantum chemistry program package. Phys Chem Chem Phys 8:3172–91
20. Frisch MJ, Trucks GW, Schlegel HB, Scuseria GE, Robb MA, Cheeseman JR, Montgomery JA Jr, Vreven T, Kudin KN, Burant JC, Millam JM, Iyengar SS, Tomasi J, Barone V, Mennucci B, Cossi M, Scalmani G, Rega N, Petersson GA, Nakatsuji H, Hada M, Ehara M, Toyota K, Fukuda R, Hasegawa J, Ishida M, Nakajima T, Honda Y, Kitao O, Nakai H, Klene M, Li X, Knox JE, Hratchian HP, Cross JB, Bakken V, Adamo C, Jaramillo J, Gomperts R, Stratmann RE, Yazyev O, Austin AJ, Cammi R, Pomelli C, Ochterski JW, Ayala PY, Morokuma K, Voth GA, Salvador P, Dannenberg JJ, Zakrzewski VG, Dapprich S, Daniels AD, Strain MC, Farkas O, Malick DK, Rabuck AD, Raghavachari J, Foresman KB, Ortiz JV, Cui Q, Baboul AG, Clifford S, Cioslowski J, Stefanov BB, Liu G, Liashenko A, Piskorz P, Komaromi I, Martin RL, Fox DJ, Keith T, Al-Laham MA, Peng CY, Nanayakkara A, Challacombe M, Gill PMW, Johnson B, Chen W, Wong MW, Gonzalez C, Pople JA (2003) Gaussian 03. Gaussian, Inc, Wallingford
21. Vreven T, Montgomery JA Jr, Peralta JE, Ogliaro F, Bearpark M, Heyd JJ, Brothers E, Kudin KN, Staroverov VN, Kobayashi R, Normand J, Raghavachari K, Rendell A, Burant JC, Iyengar SS, Tomasi J, Cossi M, Rega N, Millam JM, Klene M, Knox JE, Cross JB, Bakken V, Adamo C, Jaramillo J, Gomperts R, Stratmann RE, Yazyev O, Austin AJ, Cammi R, Pomelli C, Ochterski JW, Martin RL, Morokuma K, Zakrzewski VG, Voth GA, Salvador P, Dannenberg JJ, Dapprich S, Daniels AD, Farkas O, Foresman JB, Ortiz JV, Cioslowski JD, Fox J (2009) Gaussian 09, Revision A.02. Gaussian, Inc, Wallingford
22. Hay PJ, Wadt WR (1985) Ab initio effective core potentials for molecular calculations—potentials for K to Au including the outermost core orbitals. J Chem Phys 82:299–310
23. http://www.wavefun.com/support/sp_compfaq/Basis_Set_FAQ.html#LACVP
24. Tomasi J, Menucci B, Cammi R (2005) Quantum mechanical continuum solvation models. Chem Rev 105:2999–3093
25. Sheldrick GM (1997) SHELXTL Reference Manual. Bruker-AXS, Inc, Madison
26. Shimony-Livny I, Glusker JP, Bock CW (1998) Lone pair functionality in divalent lead compounds. Inorg Chem 37:1853
27. Arfa M, Olier R, Privat M (2008) Ab Initio calculations on the electronic structure of the divalent lead−water complex. J Phys Chem A 11(26):6004
28. Garvey JF, Herron WJ, Vaidyanathan G (1994) Probing the structure and reactivity of hydrogen-bonded clusters of the type

$\{M\}_n\{H_2O\}H^+$, via the observation of magic numbers. Chem Rev 94(7):1999
29. Kostco O, Belau L, Wilson KR, Ahmed M (2008) Vacuum-Ultraviolet (VUV) photoionization of small methanol and methanol−water clusters. J Phys Chem A 112(39):9555–9562
30. Mandal A, Prakash M, Kumar RM, Parthasarathi R, Subramanian V (2010) Ab Initio and DFT studies on methanol−water clusters. J Phys Chem A 114(6):2250–2258
31. F. DeAnglis; L. Belpassis; S. Fantacca *J. Mol. Str.* (THEOCHEM) (2009) **974**74.
32. King KA, Watts RJ (1987) Dual emission from an ortho-metalated Ir(III) complex. J Am Chem Soc 109:1589–1590
33. Wu F, Riesgo E, Pavalova A, Kipp RA, Schmehl R, Thummel RP (1999) Ruthenium(II) complexes of 2-aryl-1,10-phenanthrolines: synthesis, structure, and photophysical properties. Inorg Chem 38 (24):5620–5628
34. Clarke Y, Xu W, Demas JN, DeGraff BA (2000) Lifetime-based pH sensor system based on a polymer-supported ruthenium(II) complex. Anal Chem 72(15):3468–3475
35. Carlisle JR, Wang X, Weck M (2005) Phosphorescent side-chain functionalized poly(norbornene)s containing iridium complexes. Macromolecules 38(22):9000–9008

Supplementary material

The CIF structural file for $Ir(ppy)_2$-3,3'-Hdcbpy is available on request.